On the fatigue strength enhancement of additive manufactured AlSi10Mg parts by mechanical and thermal post-processing

Sara Bagherifard [a],*, Niccolò Beretta [a], Stefano Monti [a], Martina Riccio [b], Michele Bandini [c], Mario Guagliano [a]

[a] Department of Mechanical Engineering, Politecnico di Milano, Milan, Italy
[b] Beam-IT Spa, Fornovo di Taro PR, Italy
[c] Peen Service Srl, Bologna, Italy

Selective laser melting fabricated materials regularly exhibit excellent static strength, thanks to the very high thermal gradient that characterizes the process; however, their performance under dynamic loading is somehow restricted due to the limited ductility, tensile residual stresses, the defect density and the inadequate surface mor-phology in the as built configuration. Currently mechanical or electrochemical surface polishing steps combined with various heat treatments are integrated into the production lines to respectively address these issues. How-ever, these methods are reported to occasionally lead to inconsistent results apart from the burden of additional costs. Herein, we applied various post treatments including shot peening, sand blasting and heat treatment to evaluate their individual and synergetic effect to tackle the aforementioned challenges. Physical, microstructural and mechanical properties of SLM fabricated AlSi10Mg specimens were investigated with special focus on fatigue strength. The results highlight that appropriate post treatments can significantly enhance the fatigue perfor-mance of SLM specimens resulting in characteristics that are comparable and even better than conventionally manufactured material. Surface treatments, in particular, were found to be efficient in significantly enhancing the fatigue strength, while eliminating the necessity of polishing steps that are currently applied on as built material.

Keywords: Selective laser melting (SLM) AlSi10Mg alloy, Shot peening, Sand blasting, T6 heat treatment, Post-processing treatments

HIGHLIGHTS
•Surface treatments and T6 heat treat-ment were applied to additive manufactured parts.
•Peak hardening considerably promoted ductility and elongation.
•Fatigue properties were significantly in-creased by proper kinetic surface treat-ment.
•Post processed parts had better fatigue strength compared to conventional material.

G R AP HICAL A BSTR AC T

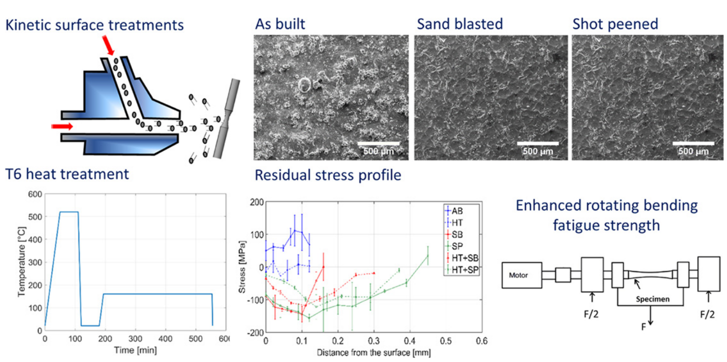

Article history:
Received 20 December 2017
Received in revised form 12 February 2018
Accepted 17 February 2018
Available online 20 February 2018

1. Introduction

With the advancement of selective laser melting (SLM) technology great attention has been devoted to assess the performance of SLM

* Corresponding author.
E-mail address: sara.bagherifard@polimi.it (S. Bagherifard).

Published Journal Article available at: https://doi.org/10.1016/j.matdes.2018.02.055

parts under static and cyclic loading for structural applications. The available literature on the structural integrity of SLM material indicates that limited ductility, the presence of tensile residual stresses caused by the complex thermal history and the rather high defect density can adversely affect the structural integrity of SLM parts, particularly under cyclic loading. Moreover, compared to conventionally manufactured components, SLM parts, exhibit high degree of surface irregularity with randomly positioned balling features or satellites along the part's periphery, mainly caused by ball form solidified material or partially melted powders [1]. Although surface roughness can be desirable for some specific applications including orthopedic implants [2–4], the poor surface quality of the as built SLM fabricated parts, can seriously deteriorate their mechanical and tribological performance, affecting also their aesthetic functions [5,6]. Poor control on surface morphology may likewise lead to limited dimensional control [7].

To address these challenges, mechanical and thermal post treatments can come into play for modulating the properties towards an improved fatigue behavior. Application of suitable heat treatments is proved to be efficient in releasing the detrimental tensile residual stresses and recovering some degree of ductility [8]. The variability of the surface roughness features are known to be highly affected by the SLM manufacturing conditions especially the orientation of the surface during fabrication [9,10]. While the effect of process parameters including scan speed, laser power and hatching distance have been studied to enhance the surface finish quality of additive manufactured parts [11–14], the resultant surfaces representing highly irregular re-entrant features are still far from ideal surface finish. To address this shortcoming, additional finishing operations including mechanical milling and machining [15,16], blasting [17,18], precision grinding and magnetic field assisted finishing [19], laser re-melting [20–22] and chemical electro-polishing [23] have been exercised. These methods often deal with other drawbacks, such as limited efficiency, inconsistency and lack of repeatability, slow application rate and environmental issues [20,24]. Besides, the efficiency of these surface polishing methods depends highly on the failure mechanism associated with the material type and on the location of the pores and defects with respect to the surface. If the pores are located within the trimmed layer of material, then polishing can highly increase the fatigue strength by totally eliminating them; whereas if the pores are brought to the surface after polishing, the fatigue performance can considerably degrade [14].

Herein, we investigate the effect of two commonly used impact surface treatments, sand blasting and shot peening, on the surface quality and fatigue performance of SLM specimens. These methods can intensely change the surface morphology without removing any material or changing the part's dimensions. Sand blasting is a mechanical surface treatment during which small media that are generally of random size and geometry are blown by pressurized air to impact the target surface. It is traditionally used at industrial scale for its simplicity to abrade scales and oxide layers from metallic component surface and mildly alter the surface roughness. Shot peening is also a mechanical surface treatment based on high energy impacts that lead to surface plastic deformation. Despite following a quite similar concept, shot peening uses highly controlled peening media regarding size, geometry, impact velocity and exposure time compared to mildly controlled sand blasting treatment. Two major parameters of Almen intensity and surface coverage [25] along with the rigorously controlled shot size and shape insure the repeatability and accuracy of shot peening treatment at industrial scale. Shot peening has been widely used to enhance the fatigue strength of metallic materials for a wide range of applications [26–30].

We also paired these mechanical surface treatments with T6 heat treatment on AlSi10Mg SLM specimens. AlSi10Mg is highly affected by precipitation hardening, since it contains both silicon and magnesium, that can cause strengthening by precipitating Mg2Si [31,32]. Considering the intrinsic differences between the microstructure of materials manufactured using conventional methods or SLM technique, it is not ideal to use the heat treatments that are tailored for conventional materials. Previous research has revealed that depending on the microstructural variations occurring during the applied heat treatment on Al alloy SLM parts, the mechanical properties can be finely controlled using proper heat treatments within a wide range to meet specific requirements [33–36]. T6 heat treatment, which consists in a solution heat treatment followed by an artificial ageing and results in stress release and peak hardening was considered as an apt option for SLM fabricated AlSi10Mg parts [16].

A large deal of effort has been put towards characterizing quasi-static mechanical behavior of the AlSi10Mg SLM parts, investigating the effect of porosity, roughness and various process parameters [37,38]. Almost all studies have reported comparable static strength of SLM specimens with that of conventionally manufactured components [37]; nevertheless, the dynamic response of as built SLM components is generally reported to be much lower than that of conventionally fabricated material. Mower et al. [24] reported a 40% rotating bending fatigue strength decrease for SLM fabricated AlSi10Mg specimens compared to the wrought material. This reduction was mainly attributed to the surface porosity, while the surface roughness of SLM specimens was also reported to be four times higher than the wrought material counterparts. Siddique et al. [39] identified the action of subsurface pores combined with surface roughness as the main cause of favored crack nucleation and reduced fatigue strength for AlSi10Mg as built specimens. They recommended re-melting contour zones as a scan strategy to decrease pore density near the surface and thus improve the performance of fatigue loaded components [39]. Surface machining has been reported to have a decisive role in enhancing fatigue strength of SLM fabricated AlSi10Mg material to comparable or even higher values than materials manufactured by traditional processes [40].

While there are clear indications of favorable effects of heat treatment on fatigue performance of AlSi10Mg SLM parts [8,40], there are very few studies that apply impact based surface treatments in the field of additive manufacturing. Book and Sangid [41] studied the layer by layer in situ application of shot peening to direct metal laser sintering (DMLS), which resulted in just slight changes in the surface appearance of the AlSi10Mg specimens. The results were mentioned to be inconclusive likely due to insufficient surface coverage. Another study investigated the effect of shot peening on surface roughness, compressive yield strength, and wear resistance of DMLS fabricated stainless steel [42]. The grain refinement induced by shot peening was mentioned to be the main cause of enhanced properties. However, while notable grain refinement can be obtained by raising the kinetic energy of the process, the extremely limited grain refinement induced by conventional shot peening is implausible to affect the general properties of the treated material [27,43–45]. Wycisk et al. [46] investigated the tension-tension ($R = 0.1$) high cycle fatigue strength of as built, polished and shot peened Ti6Al4V SLM specimens. Their results revealed a remarkable improvement of fatigue strength with respect to the as built condition, which was still lower than that of wrought material. Wycisk et al. [46] mentioned the shot peening results to be incompatible with the data obtained for polished specimens possibly due to the nucleation of cracks from sub-surface layers [46]. With the exception of [46], to the best of the authors' knowledge, there is no study investigating the effect of sand blasting or shot peening on the microstructural, physical and mechanical properties of additive manufactured parts. To come to the point, the application of kinetic impact-based surface treatments in the field of additive manufacturing is mostly limited to inconclusive reports for sintering based manufacturing techniques. Moreover, in the existing studies, the terminology and even the apparatus of sand blasting and shot peening have been used interchangeably, neglecting the intrinsic differences between the two treatments. In most cases, the effect of the applied treatment is studied just on the surface roughness parameters, ignoring its effect on mechanical properties [47]. These matters lead to a highly inconclusive current state of the art regarding application of impact based surface treatments to additive manufacturing field. The present research evaluated the potential of impact based surface treatments paired with T6 heat treatment to be used as a substitute to the commonly used polishing phase; these surface treatment are expected to improve the surface quality of SLM fabricated AlSi10Mg parts while also bringing in a considerable prospective fatigue strength enhancement. Particular attention was focused on the high cycle fatigue strength after individual post-processing treatment as well as their combination to investigate the synergic effects. The obtained results were compared with those of the material fabricated using conventional manufacturing methods.

2. Materials and methods

2.1. Specimen preparation

Gas atomized AlSi10Mg powder (SLM solutions Group AG, DE) (Fig. 1a) with an average diameter of 50 μm and nominal chemical composition reported in Table 1 was used for SLM specimens.

The specimens were manufactured using a SLM 500HL system (SLM Solution Group AG, DE) that is characterized by a build chamber of 280x500x350 mm^3 and four Yttrium fiber lasers that work simultaneously. The process parameters were set to laser power of 350 W, scan speed of 1150 mm/s, spot diameter of 78 μm, layer thickness of 50 μm and hatch distance of 0.17 mm, resulting in a fluence of 35.81 [J/mm^3]. The mechanical properties of SLM parts are significantly affected by the fabrication parameters including baseplate pre-heating temperature, laser power, hatch distance, building direction, etc. [48,49]. Herein, the specimens were fabricated in vertical direction using a scanning strategy of 67° rotation between the subsequent layers and the contour zone was re-melted every time, before depositing the successive layer. Considering the anisotropy induced by build direction, this condition was selected to consider worst-case scenario in terms of mechanical strength. The four lasers working in parallel divided the building platform into seven areas; in four of which only one laser was operational, whereas, in the other three, two lasers alternate (Fig. 2). The latter build areas are hereafter called overlapping regions.

Reduced thermal gradient obtained by baseplate heating is reported to decrease the porosity and the required heat input for powder melting, thus providing the possibility of increasing the scan speed without compromising the deposition density [50]. Accordingly, the platform was heated to 150 °C and the chamber was flooded with argon, keeping the oxygen content below 0.2%. At the end of the deposition process, the specimens were detached from the platform using wire electrical discharge machining. Two different specimen geometries, reported in Fig. 1c, were used in the experiments. Dog bone specimens were considered for tensile tests and hourglass specimens for fatigue tests following ASTM E8/E8M-16a and ASTM E466-15 respectively. Cubic specimens were considered for the rest of the experiments unless specified.

Table 1
Chemical composition of AlSi10Mg powder provided by the supplier.

Element (wt%)	Al	Si	Fe	Cu	Mn	Mg	Zn	Ti
Minimum	Balance	9.0	–	–	–	0.2	–	–
Actual	Balance	9.8	0.24	<0.005	<0.005	0.44	<0.002	<0.01
Maximum	Balance	11	0.55	0.05	0.45	0.45	0.1	0.15

2.2. Post processing

Sand blasting was performed manually at a pressure of 0.7 MPa with a stand-off distance of 20 cm for 40 s using micro-sphere glass medium with a diameter range of 200–300 μm. Here, we adopted a more severe and rather controlled sand blasting treatment compared to what is commonly used in the industry, in order to elevate its effect on surface roughness of the SLM fabricated parts. Shot peening was implemented using steel S170H medium (0.43 mm diameter), Almen Intensity of 10 A [0.001 in.] to a full surface coverage. T6 thermal treatment was performed following the interval times and temperature range recommended in [51]. The final quenching step was performed in water following the work of Gharavi et al. [52]. As described in Fig. 1b, the T6 heat treatment consisted in heating up to 560 °C, solution heat treatment for 1 h, quenching in water (−160 °C/min) with a storage time of 1 h, followed by heating up to 160 °C (10 °C/min) and ageing for 6 h at 160 °C, concluded by final quenching in water.

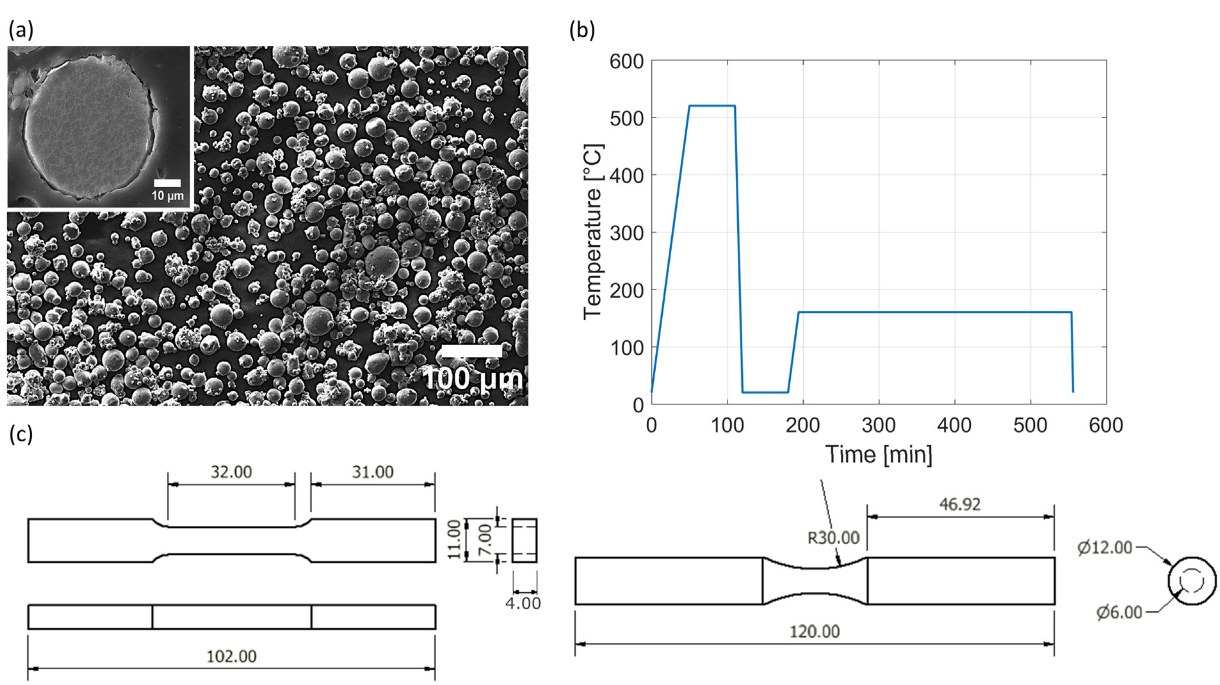

Fig. 1. a) SEM micrograph of the powders' morphology with the insert corresponding to the microstructure of a single powder particle b) the applied T6 heat treatment c) dog bone and hourglass specimens used for tensile and fatigue tests (all dimensions are in mm).

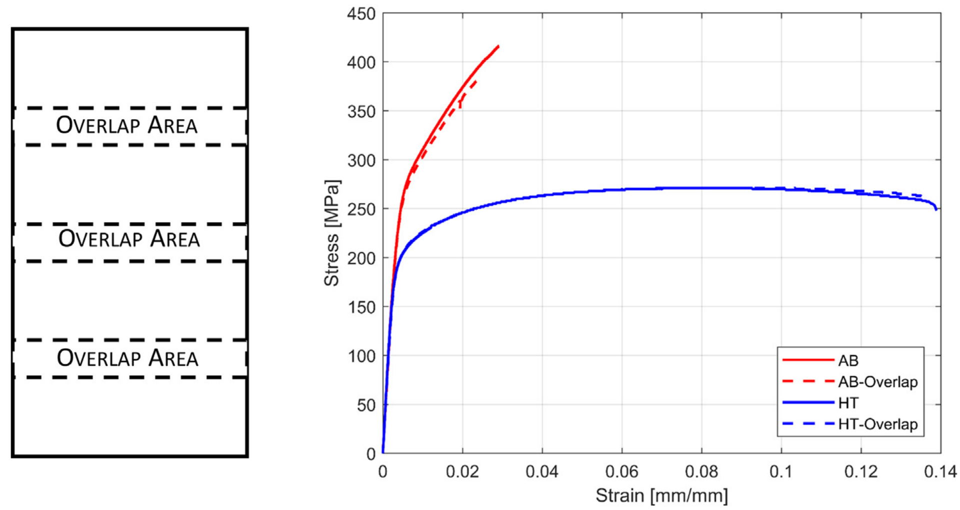

Fig. 2. Monotonic engineering stress-strain curves for AB and HT series separating the data for specimens built in non-overlap and overlap area (AB: as built, HT: heat treated).

Six different sets of specimens were considered in order to investigate the sole effect of each post treatment as well as their synergistic influence on mechanical and physical properties of the SLM specimens. The studied series include as built (AB), heat treated (HT), sand blasted (SB), shot peened (SP), heat treated + sand blasted (HT + SB) and heat treated + shot peened (HT + SP).

2.3. Tensile strength test

Monotonic tensile tests were carried out on as built and heat treated series, each consisting of six specimens. Each series included three specimens built in the non overlapping zone, and three in the overlapping zone of the build area, to assess the effect of laser overlapping on quasi-static response. The specimens were tested following ISO 6892-1 on an MTS Alliance RT/100 machine at a strain rate of 0.7 mm/min up to 2% strain followed by a constant rate of 2 mm/min. An extensometer was attached to the specimens to measure the material elongation during the experiment.

2.4. Microstructural characterization

Longitudinal and transversal sections of specimens were impregnated in hot mounting resin. The grinding steps were carried out with graded emery papers followed by final polishing steps using water based polycrystalline diamond suspensions up to an average scratch size of 1 μm. The polished cross sections were chemically etched for 20 s in Keller's reagent (95% pure H_2O, 1% HF, 1.5% HCl, 2.5% HNO_3). Powder particles were also impregnated in cold mounting resin and gone through grinding, polishing and chemical etching steps (insert in Fig. 1a). The etched cross sections were observed in bright field using Leitz Aristomet optical microscopy and a Zeiss EVO 50 scanning electron microscopy (SEM).

2.5. Porosity measurement

The specimens were rinsed ultrasonically in acetone and then in distilled water for 10 min each. Multiple SEM micrographs were taken from random areas of polished cross sections in backscattered electron (BSE) mode. ImageJ software [53] was used to analyze the SEM images. The BSE-SEM images where binarized setting a threshold value and the porosity was estimated as the ratio of the black to white pixels that signified the fraction of the pores surface over the total area. The average pore size was calculated using particle analysis option in ImageJ software. Image analysis provided reliable information about the matrix porosity; however, to include the effect of surface treatments and thus the possible variation of porosity close to the surface area, a second porosity evaluation method based on Archimedes buoyancy principle was considered. This latter, was performed using an electronic balance (Precisa 100 A–300 M) density Kit to compare the weight of the specimens in water and air and compute the overall density. Specimen's overall porosity was calculated by comparing density Kit results with the base material density, considering a full density of 2.68 g/cm^3 for AlSi10Mg, provided by the powder supplier.

2.6. Surface roughness measurement and morphology observation

Surface roughness was measured using a Mahr Perthometer (PCMESS 7024357) equipped with MFW-250 probe with a tip diameter of 5 μm. Sampling and cut-off lengths and the filtering technique were all set according to EN ISO 4287 standard. Two specimens were considered for each series and three measurements were carried out on random zones of each specimen. Average values of standard roughness parameters including arithmetic mean of the absolute ordinates from the reference line of the roughness profile (R_a), root mean square of the ordinates from the reference line of the roughness profile (R_q), sum of the largest peak height and the largest valley depth within the evaluation length (R_t) and the mean of the five R_t values from the five sampling lengths considered within the evaluation length (R_z) are reported for each series.

The surface morphology of specimens was studied using a Zeiss EVO50 SEM. Energy dispersive X-ray (EDX) analysis was used to analyze the composition of some surface agglomerates. For both surface roughness measurements and morphology observations, the specimens were ultrasonically cleaned in acetone for 15 min, beforehand.

2.7. Microhardness measurement

Microhardness tests were performed on specimen's polished cross sections using a Leica WMHT30A micro Vickers hardness tester. Indentations were produced using a load of 50 gf and dwell time of 15 s along three parallel paths starting from the surface towards the core material on specimens' transversal section (i.e. perpendicular to the build direction) for each series to present average data at each specific distance from the surface.

2.8. Residual stress measurement

X-ray diffraction was used to obtain the in-depth distribution of residual stresses along a path perpendicular to the build direction on

Table 2
Monotonic mechanical properties for SLM specimens compared with conventionally cast material.

	AB	HT	Conventional cast and aged (EN1706 and [37])
Young modulus (GPa)	72 ± 1.5	73 ± 1	71
Yield stress (MPa)	273 ± 3	201 ± 6	180
Ultimate stress (MPa)	393 ± 20	265 ± 9	300–317
Elongation at fracture (%)	2.5 ± 0.4	13 ± 1	2.5–3.5

different series of specimens. AST X-Stress 3000 portable X-ray diffractometer (CrKα radiation (λK alpha 1 = 2.2898 Å)), $\sin^2(\psi)$ method, was used at a diffraction angle (2θ) of 139° corresponding to 311-reflex scanned with a total of 7 tilts in the range of −45° to 45° along three rotations of 0°, 45° and 90° with constant step size of 0.028°.

Electro-polishing was applied for step by step material removal on a circular area with a diameter of 0.5 cm^2 using an electrolytic solution of 94% CH_3COOH, 6% $HClO_4$ at a voltage of 35 V. A precision Mitutoyo micrometer (IDCH0530/05060) was used to insure that the depth of the path increased by 0.02 mm at each removal step.

2.9. Fatigue tests and fractography analysis

Room temperature rotating bending fatigue tests (stress ratio (R) = −1) were carried out on hourglass specimens following the stair-case method [54] with a steps size of 10 MPa on different series each consisting of 15 specimens. Italsigma (IT) machine was used at a rotational speed around 2000 rpm. Fatigue strength corresponding to three million cycles was computed using both Hodge-Rosenblatt method [55] and the statistical approach suggested in ISO12107. Fracture surface analysis was carried out on failed specimens using a SteREO discovery V12 Zeiss optical microscope first to have general traits of crack initiation and propagation zones. Subsequently the specimens were further analyzed by Zeiss EVO50 SEM.

2.10. Statistical analysis

For all the reported experimental data, the reported arithmetic means and standard deviations refer to averages of three independent measurements, unless specified. The t-student test was used to determine statistical significance between different series.

3. Results

3.1. Tensile test

Fig. 2 showing representative stress-strain curves for AB and HT specimens taken from both overlap and non-overlap zones of the build area, exhibit no noteworthy effect of multiple laser beams concurrently working on the build area. The average data of the three specimens tested for each series summarized in Table 2, confirm that the responses of AB and HT specimens to quasi-static tensile loading are independent from laser overlapping. In the light of this observation, hereafter, the data are reported regardless the number of laser sources involved in the fabrication of specimens.

Tensile test results indicated a notable difference between the quasi-static mechanical properties of the specimens before and after heat treatment, highlighting a significant increase in the elongation along with ultimate tensile strength reduction. All SLM specimens exhibited an elastic modulus comparable with that of the conventionally manufactured cast material reported in EN1706 and [37] combined

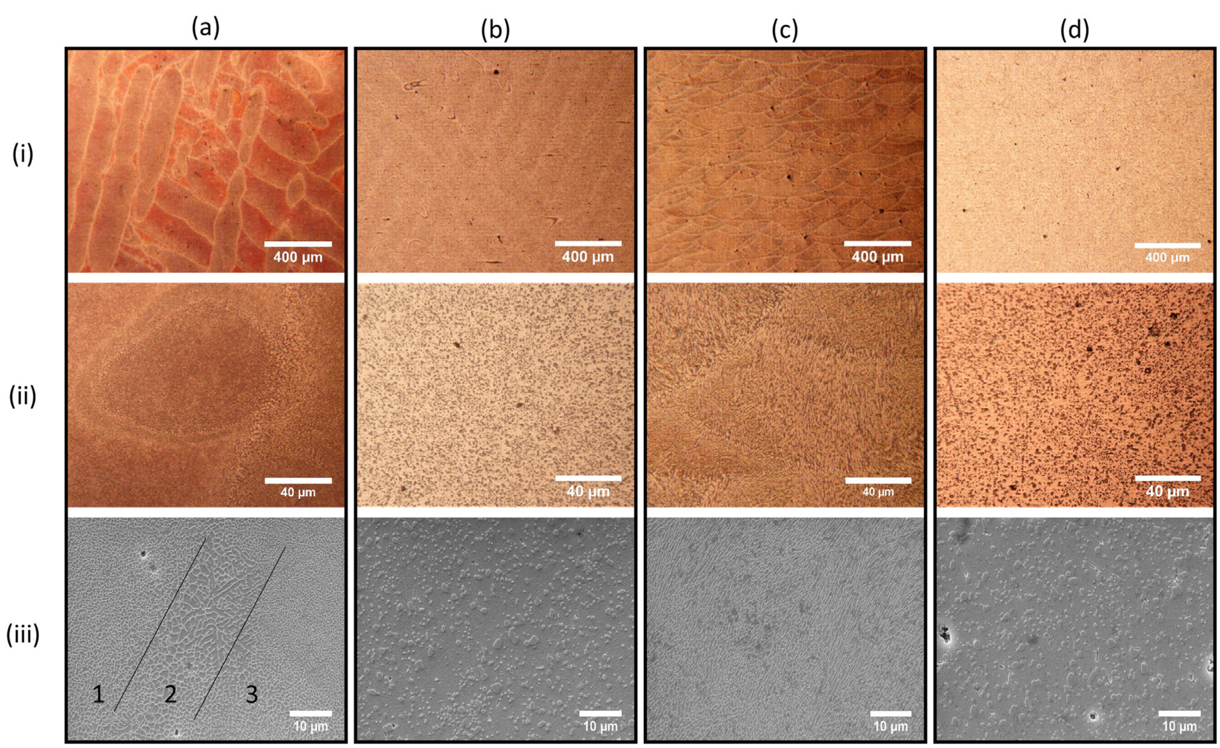

Fig. 3. Optical and scanning electron microscope images of (a) AB transversal section (b) HT transversal section (c) AB longitudinal section (d) HT longitudinal section (AB: as built, HT: heat treated).

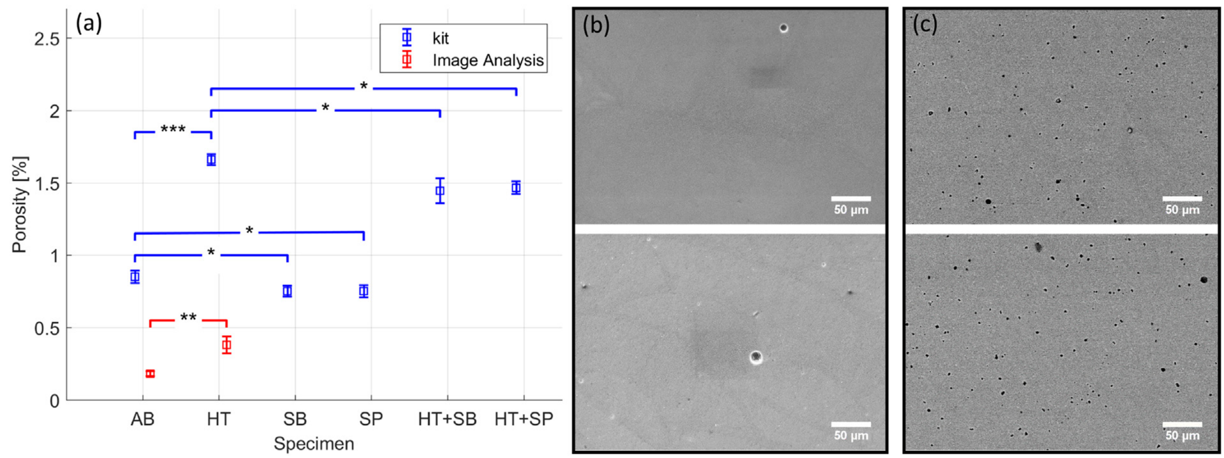

Fig. 4. a) Porosity measurement obtained through image analysis and density Kit; N = 3 *$p < 0.05$, **$p < 0.01$ and ***$p < 0.001$. BSE-SEM micrographs showing the size and distribution of pores b) AB transversal (top) and longitudinal (bottom) sections c) HT transversal (top) and longitudinal (bottom) sections (AB: as built, HT: heat treated).

with higher yield and ultimate tensile strength. The elongation of the AB series is also comparable with that of the cast material; however, the HT specimens represented five times higher ductility.

The applied surface treatments (sand blasting and shot peening) are not expected to affect the static tensile behavior as they affect just a thin layer of material on the periphery of the specimens. In order to confirm this notion, SB series were tested before and after heat treatment. The results, presented in Supplementary data (Fig. S1), matched very well with that of the AB specimens.

3.2. Microstructural analysis

SEM micrograph of the polished and chemically etched powder cross sections presented in Fig. 1a highlights the original powder microstructure characterized by the presence of eutectic silicon particles (bright phase) segregated at the boundaries of α-Al grains (dark phase). The cross sectional observation of the powder also shows no internal defects in the inner dendrite structure.

The microstructure of specimens' transversal (perpendicular to the build direction) and longitudinal (parallel to the build direction) cross sections for AB and HT specimens are presented in Fig. 3. The transversal section of AB specimen (Fig. 3a(i)) portrays the molten pools along the laser scanning direction showing also the underneath layers formed at different orientations caused by the scanning strategy, which is 67° rotation between subsequent layers. Higher magnitude observation in Fig. 3a(ii) reveals a notably inhomogeneous microstructure for AB transversal section exposing coarser microstructure at molten pool boundaries compared to the inside zones. In particular, the SEM micrograph of the transversal cross section of AB corresponding to two adjacent molten pools exhibits the presence of three distinct zones with dissimilar grain structure, Fig. 3a(iii). In the cellular-dendritic structure of the differently affected zones, zones 1 and 3 correspond to the molten pools with quite fine microstructure, whereas zone 2 refers to the region with coarser structure on the molten pool contour.

After the heat treatment, the molten pools and laser traces become almost invisible in the transversal cross section (Fig. 3b(i)). Significant homogeneity is achieved (Fig. 3b(ii)) as the segregated Si around α-Al grains, diffuses to form particles that are homogeneously dispersed in the α-Al matrix. In addition, the T6 heat treatment not only resulted in particle diffusion at grain boundaries, but as also reported in [56], led to the formation of rod formed (needle like) Mg2Si precipitates, which are highlighted in figure Fig. 3b(iii) together with the randomly distributed silicon particles within the α- Al matrix.

The longitudinal cross section of the AB specimen, (Fig. 3c(i)) presents semicircular laser traces caused by the Gaussian distribution of the laser beam [57]. An individual molten pool presented at higher magnification in Fig. 3c(ii) indicates columnar dendrites along the building direction and highlights coarser microstructure in the contour zone

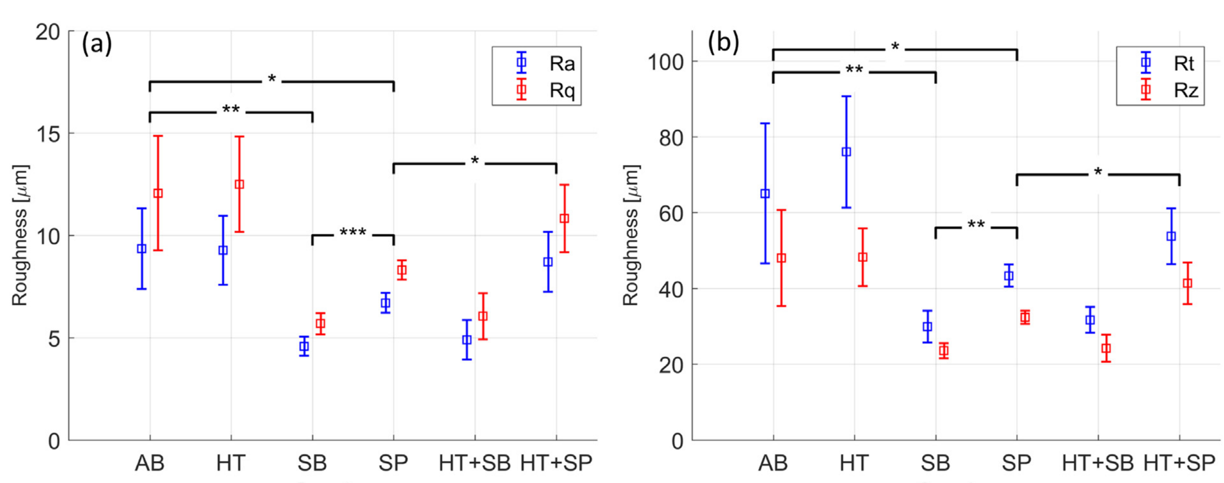

Fig. 5. Microscale surface roughness parameters *$p < 0.05$, **$p < 0.01$ and ***$p < 0.001$ (AB: as built, HT: heat treated, SB: sand blasted, SP: shot peened, HT + SB: heat treated and sand blasted, HT + SP: heat treated and shot peened).

(molten pool interfaces). The columnar dendrites along the building direction are even more evident in Fig. 3c (iii). Microstructural homogenization, dendrites elimination, and the scattered distribution of silicon particles can be observed in the longitudinal cross section after heat treatment (Fig. 3d), similar to the observations in Fig. 3b.

The cross sectional observations of SB and SP series (presented in Fig. S2) exhibited no notable difference between the microstructure of the near surface and inside matrix.

3.3. Porosity

The results of measurements performed on different sets of specimens using both image analysis of BSE-SEM micrographs and the density Kit are reported in Fig. 4a. The results obtained from these two methods are not directly comparable, as image analysis offers a cross sectional evaluation whereas density Kit refers to volume porosity; however, they present similar trends between different series. Image analysis evaluates mainly the core material porosity and thus was carried out just on AB and HT specimens considering the insignificant effect of surface treatments on matrix porosity. The porosity data, in general, indicate notable porosity increase after heat treatment (Fig. 4 b–c). Sand blasting and shot peening have almost the same porosity in all configurations (applied before and after heat treatment) and both seem to cause a slight reduction of porosity with respect to the AB condition. Image analysis of multiple micrographs confirmed similar size (up to 10–12 μm) of the pores in longitudinal and transversal section for both AB and HT series, indicating that maximum pore size does not increase after heat treatment. It is worth noting that in all cases the pores did not seem to be particularly localized in the sub-surface area.

3.4. Surface roughness and morphology

Fig. 5a and b report the average roughness data on all series. As expected, AB and HT specimens exhibit similar surface roughness, which are quite higher than that of the surface treated series. Besides, measurements on AB and HT specimens were characterized by a quite high scatter considering the randomly located surface irregularities. The sand blasted specimens (SB and HT + SB) show quite similar roughness that are the lowest among all series. Whereas SP specimens represent higher surface roughness, that is further increased on the HT + SP specimens. Similar trends are observed for variation of all roughness parameters among different series.

SEM observations presented in Fig. 6 provide qualitative comparison of the specimens' top surface morphologies. The AB and HT specimens displayed a very irregular surface, characterized by randomly unmolten powder particles often forming agglomerates that lead to the high surface roughness reported in Fig. 5. Sand blasting strongly decreased imperfections on the surface reducing notably the number of the irregularities. However, few unmolten powder particles, which were partially incorporated within the specimen's surface by the impacting media, could be still observed on the surface of SB series (insert in Fig. 6(c)). EDX analysis confirmed that the incorporated particles were effectively unmolten powders of AlSi10Mg. The SP series represented a similar but more regular surface state compared to that of SB ones with clearly wider surface dimples and indentations caused by the higher kinetic energy of the shot peening treatment. The effect of mechanical surface treatments on the heat treated specimens were more evident, inducing more apparent dimple boundaries on the treated surfaces. Also in this case, HT + SP series exhibited wider dimple arrangements compared to the HT + SB series.

3.5. Microhardness

Microhardness data presented in Fig. 7a indicate that AB and HT specimens represent an almost constant trend along the depth respectively corresponding to microhardness of 130 and 85 HV; whereas SB and SP series exhibit a higher value close to the surface caused by the work hardening effect generated by the impacts. SB specimens induced a work hardening effect of about 10% increase on the surface layer, which gradually decreased reaching to the core material hardness at a depth of about 100 μm. SP specimens, on the other hand, exhibited a higher hardness increase of about 20% on the surface, and a deeper affected layer of about 200 μm. A similar trend was observed for the HT + SP and HT + SB series presenting quite the same surface hardness increment with respect to the HT specimen (respectively about 10% and 20%), and a slightly higher depth for the affected layer (around 125 μm and 250 μm respectively) compared to SB and SP specimens. It is interesting to note that the AB specimens exhibited a much higher hardness compared to that of the bulk material manufactured using conventional techniques [37], while the HT specimens had comparable hardness with conventional material.

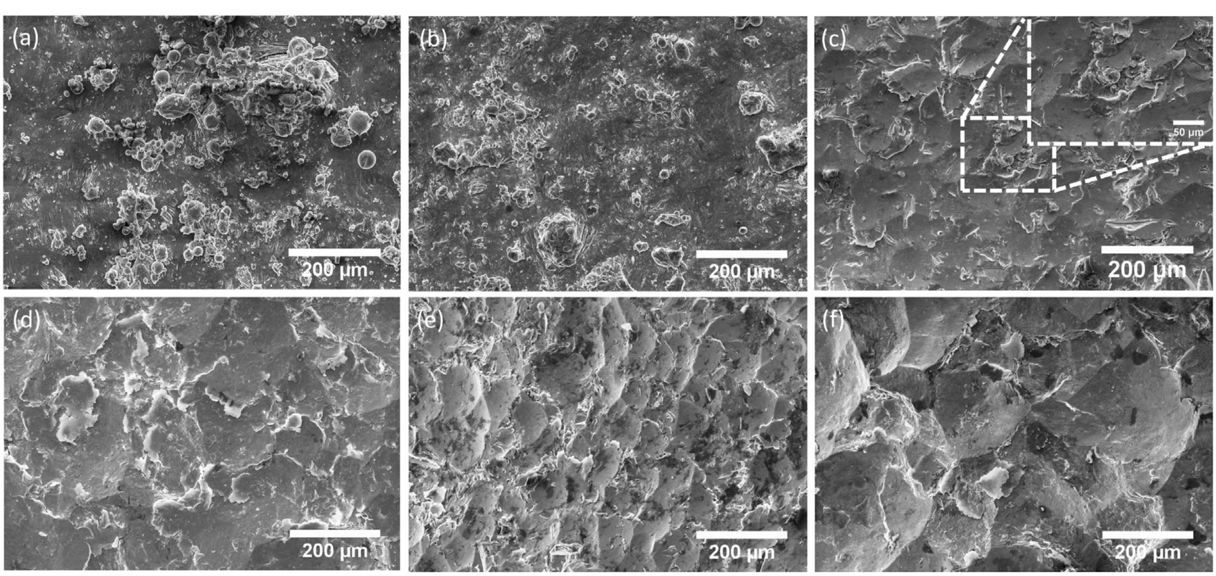

Fig. 6. Top surface SEM micrographs of a) AB b) HT c) SB d) SP e) HT + SB f) HT + SP (AB: as built, HT: heat treated, SB: sand blasted, SP: shot peened, HT + SB: heat treated and sand blasted, HT + SP: heat treated and shot peened).

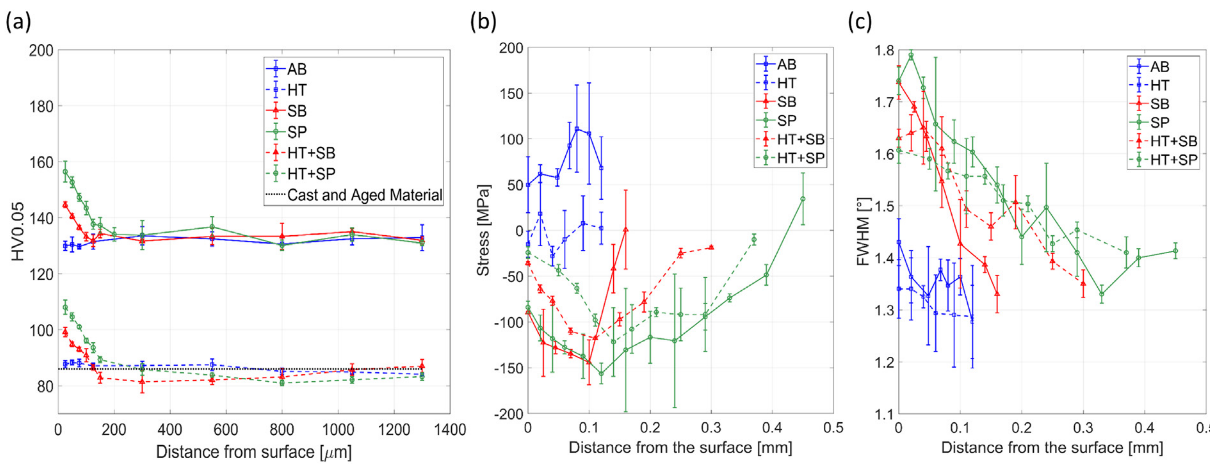

Fig. 7. a) Microhardness data of SLM specimens compared with conventional cast and aged material [37] b) distribution of residual stresses and c) distribution of FWHM as a function of the distance from the surface (AB: as built, HT: heat treated, SB: sand blasted, SP: shot peened, HT + SB: heat treated and sand blasted, HT + SP: heat treated and shot peened).

3.6. Residual stress analysis

The in-depth profile of residual stresses and FWHM parameter are reported in Fig. 7b and c. AB specimens presented a rather constant tensile residual stresses with an average of about 70 MPa. This stress distribution was completely relaxed after the heat treatment. SB and SP specimens demonstrated the typical trend of residual stresses induced by impact based surface treatments [58], representing on-surface stresses of about −90 MPa, which continuously increased in magnitude to reach a peak value of around −145 MPa at the depth of 0.1 mm and −155 MPa at the depth of 0.12 mm respectively for SB and SP series. The residual stresses then decreased until reaching tensile values. The profile of residual stresses for SB specimen held a very high gradient, with a total depth of 0.16 mm affected by compressive residual stresses, while the SP series exhibited a much higher affected depth of 0.42 mm.

When applied after heat treatment, the kinetic surface treatments represented lower on-surface residual stresses compared to not heat treated series. The maximum stress was detected at roughly similar depths compared to the respective not heat treated series (0.11 mm and 0.14 mm for HT + SB and HT + SP respectively) and a higher total depth of layer affected by compressive residual stresses of 0.3 mm and 0.36 mm were detected respectively for HT + SB and HT + SP specimens.

Regarding FWHM parameter, the AB and HT specimens showed an almost constant profile along the depth, with slightly lower values for HT series. Higher surface values were measured for SB and SP specimens; in both cases, a gradually decreasing trend is observed by going in depth; although the SB specimen demonstrated a much higher gradient to reach the FWHM of the core material compared to SP series. HT + SB and HT + SP showed comparable FWHM on the surface that is lower than that of the SB and SP series.

Table 3
Fatigue strength corresponding to 3 million cycles for all series.

Sample series	Fatigue strength (Hodge-Rosenblatt) (MPa)	Fatigue strength (ISO12017) (MPa)
AB	36	50 ± 4
HT	83	75 ± 7
SB	161	173 ± 4
SP	176	185 ± 13
HT + SB	162	175 ± 4
HT + SP	101	102 ± 4
Cast A360-T6 [59]	(depending on the casting process)	76–115 ± 10
Wrought 6061 alloy [24,61]		120

AB: as built, HT: heat treated, SB: sand blasted, SP: shot peened, HT + SB: heat treated and sand blasted, HT + SP: heat treated and shot peened.

3.7. Fatigue

Fatigue strengths corresponding to 3 million cycles, estimated following both Hodge-Rosenblatt [55] and the statistical approach suggested by ISO12107 standard are reported in Table 3. The fatigue strength of SLM fabricated specimens is compared also to the fully reversed rotating bending fatigue strength of die-cast A360 for 2 million cycles [59], considering the similar chemical composition to A360 aluminum casting alloy to that of AlSi10Mg [60]. For comparison, also the fatigue test data of Al6061 alloy is reported in Table 3. Al6061 is one of the most widely used aluminum alloys particularly in aerospace application and is commonly sourced in the literature as conventionally manufactured material for comparison with SLM fabricated Al material [24].

The heat treatment considerably improved the poor fatigue performance of AB series. Surface treatments further increased the fatigue strength, with the highest strength obtained for SP series. After heat treatment, sand blasting did not further enhance fatigue strength compared to the SB series and it was found to be more effective compared to HT + SP treatment.

3.8. Fractography analysis

The overall view of a representative fracture surface of AB specimen (Fig. 8a(i)) points out a primarily smooth surface indicating stable propagation of multiple surface cracks along different planes, which later merge together leading to the final fracture. A surface crack initiation site is shown in Fig. 8a(ii); sub-surface porosities seem to have influenced the crack propagation path (Fig. 8a(iii)). The limited final rupture zone, corresponding to unstable crack propagation (Fig. 8a(iv)) exhibits by and large few dimples formed features that highlight the limited ductility of the AB specimen.

Fig. 8b shows the representative fracture surface of a HT specimen. Unlike AB series, the striation lines that are characteristic features of stable crack propagation are quite visible (Fig. 8b(i)). SEM observations indicate the propagation paths of multiple cracks nucleated from the surface irregularities (Fig. 8b(ii)). The zone of fast fracture, presented in Fig. 8b(iii) exhibits a clearly ductile behavior, characterized by the prominent presence of dimples (Fig. 8b(iv)).

The presence of fish-eye crack could be easily distinguished on the fracture surface of SB specimens (Fig. 8c(ii)), at the center of which normally a pore or a small defect could be detected; the outer circular region represented the crack propagation in a pattern that radiated away from the central defect (Fig. 8c(iii)). Fig. 8c(iv) shows the boundary between different regions representing the change of the crack growth mechanism during propagation.

Fig. 8d portrays a representative fracture surface of a SP specimen. The smooth region at the bottom part of the fracture surface corresponds to the stable crack propagation (Fig. 8d (ii)) starting from a surface-nucleated crack. Fig. 8d(iii) represents the initiation site of the dominant crack, the propagation of which has been affected by sub-surface porosities. The final fracture zone, highlighted in Fig. 8d (iv), represents brittle features with presence of no dimples; the bright color can be due to the slanted fracture surface caused by the coalescence of multiple cracks.

Fig. 8(i)e reports the overall view of fracture surface of a HT + SB specimen. Multiple crack initiation sites were observed on the fracture surface, some of which are shown in Fig. 8e (i)–(iv). There seemed to be no dominant crack, as several cracks propagated in a stable manner resulting in stirations towards the inner part of the specimen. The final fracture occurred at the center of the cross section, leaving behind dimples indicating a ductile fracture similar to the HT specimens.

Fig. 8f represents the fracture surface of a HT + SP specimen. Similar to SP specimen, the nucleation site of a dominant crack could be noticed on the surface, the stable propagation of which resulted in slight striations towards the bulk material (Fig. 8f(ii)). Final rupture zone that corresponds to unstable crack propagation is characterized by the presence of dimples (Fig. 8f (iii)). It is worth noting that the dominant crack

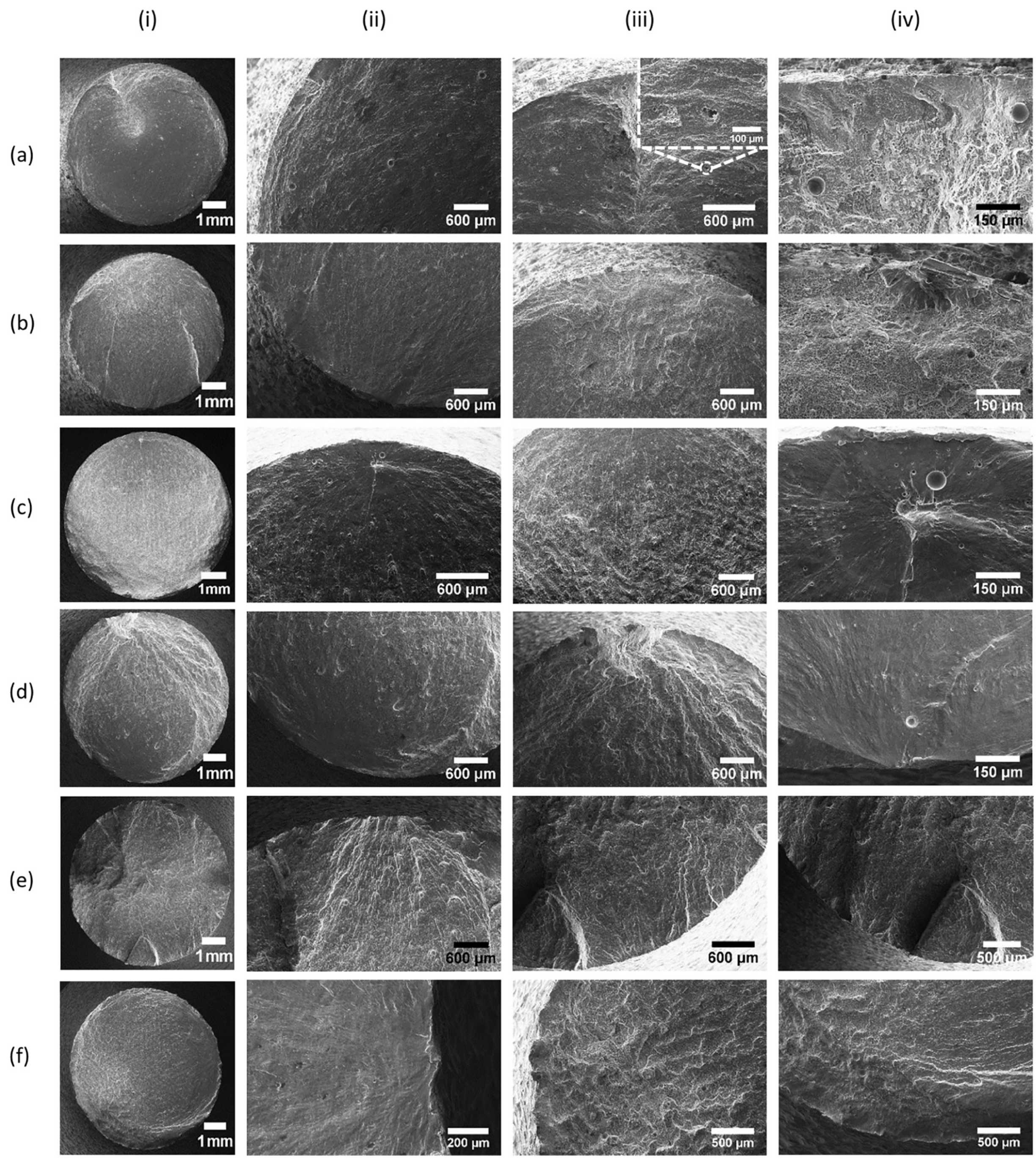

Fig. 8. SEM observation of the fracture surface of a) AB b) HT c) SB d) SP e) HT + SB f) HT + SP specimens (AB: as built, HT: heat treated, SB: sand blasted, SP: shot peened, HT + SB: heat treated and sand blasted, HT + SP: heat treated and shot peened).

tended to propagate in the interfaces between scan tracks, as they are clearly visible in Fig. 8f(i) and (iii). Due to the presence of a dominant crack the fracture primarily occurred along a single plane; however, the presence of other small cracks could have led to the formation of a slightly sloped fracture surface, represented in figure Fig. 8f(iv).

4. Discussion

Tensile test data showed no significant difference between the specimens built in overlap and non-overlap areas. Thus, it can be concluded that using two lasers that alternate on the build area can optimize the building time without compromising the resultant mechanical properties.

The comparable or even superior yield and ultimate tensile strength of AB specimens compared to cast and aged material, as reported also in [37,62], can be attributed to the fine grain size assured by the high cooling rates of the SLM process. The applied heat treatment reduced the ultimate tensile strength by over 30%; on the other hand, it led to over 400% elongation enhancement. The grain coarsening that occurred during heat treatment can be responsible for the observed trend that is justified following the Hall-Petch equation [62]. HT specimens showed a tensile strength that is just slightly below the conventionally manufactured material, while representing much improved ductility.

The microstructural observation of AB specimen's longitudinal and transversal cross sections indicated an anisotropic microstructure evidently representing laser scan tracks. The inhomogeneity of the cellular-dendritic microstructure in AB configuration was more apparent in SEM micrographs where much finer structure was observed at molten pool's center compared to its contour area. In Fig. 3a (iii), as the molten pool in zone 1 solidified, the laser melted the adjacent zone 3 in a subsequent pass; therefore, the fusion contour zone 2 was subjected to a longer exposure time, which led to formation of coarser microstructure [38,63]; while the neighboring areas that have a higher cooling rate represent a finer microstructure [64]. After heat treatment, molten pool and laser scanning traces disappeared and the microstructure tended to become homogeneous, representing quite the same features in both longitudinal and transversal directions. This observation is in agreement with the report of Brandl et al. [8], describing the role of T6 heat treatment on microstructural homogenization, where interdentritic Si particles become spherical, needle like Mg2Si hard phase precipitations occur and the heat affected zones and laser traces are eliminated. SEM observations of the longitudinal cross section of AB specimen, confirmed that the Si particles, which were originally segregated at α-Al boundaries (Fig. 3 a), diffused in the matrix; thus they were no more confined around α-Al grain boundaries after heat treatment. This homogenization that is supposed to start during the solution heat treatment and continue during ageing phase [56], is expected to uphold the elimination of mechanical properties dependence upon the building direction [8].

The quite high cooling rates and the rapid solidification during SLM process can be unfavorable for degassing and thus may enhance the pore formation risk [65]. The presence of pores that may act as stress raisers can highly affect the performance of the structure under static and cyclic loading, depending on the size and position of the pores with respect to the external surface. The porosity measurements indicated that heat treatment notably increased the specimens' porosity. We repeated the measurements several times for each series and the low scatter of the data confirmed the repeatability of the measurements. The variability of porosity between the samples of the same series was found to be very low and the T-student test between mean values, revealed statistically significant difference between the two as built and heat treated series. This observation can be attributed to the increased specific volume of the trapped air within the material matrix upon heating that led to pores expansion. This effect, which was reported also by Siddique et al. [63], arises until an equilibrium is reached between the resistance force of the material and the force exercised by the expanded air. Thus, the pressure developed inside the pores because of increased temperature can push the inner walls of the pores, until volume expansion allows us to accommodate the increase in pressure [63]. The image analysis data indicated that the critical condition, for which equilibrium was reached and the pore diameter did not further increase, is about 10–12 μm, that is the maximum pore size observed in the SEM micrographs. The reduced porosity after kinetic surface treatments can be acknowledged as a result of the multiple shot impacts and the high extent of plastic deformation on the top surface layer that tended to close the surface pores. Similar occurrence was reported by Manfredi et al. [66] who observed slight porosity reduction after application of shot peening to DMLS parts.

Surface roughness is known to play a significant role in fatigue performance particularly under full reversal loading, where the maximum stress is applied to the surface layer and thus surface irregularities and the presence of subsurface porosities are more likely to lead to fatigue crack nucleation. The high surface roughness and the notable scatter of roughness data for AB and HT series are due to the non-homogeneous surface morphology. The kinetic energy of the impacting media tended to eliminate the unmolten powder particles and surface agglomerates and reduced the surface roughness respectively by 50% and 30% for SB and SP compared to AB series. The higher surface roughness of HT + SP compared to SP specimens might be due to the high impact energy of shot peening that resulted in formation of more pronounced dimples and indentations on the softened material after by heat treatment. This observation can suggest that, if the surface treatment is characterized by sufficiently high impact energy, a decreased hardness of the material can lead to much accentuated surface indentations and thus higher surface roughness. It is also worth noting that, unlike sand blasting, the primary application of shot peening is not to reduce surface roughness, but to induce compressive residual stresses, work harden and modify surface layer microstructure [43,45]. Provided that proper shot peening parameters are used, these aspects can compensate for the effect of surface roughness [67].

Surface morphology of the AB specimens exhibited a high density of isolated surface agglomerates. Sand blasting reduced the number of surface pinpointed irregularities and shot peening totally eliminated them. The treated surfaces were characterized by multiple overlapping indentations generated by the multiple impact. Higher kinetic energy of the shot peening treatment resulted in wider plastic indentations as well as creased and crumpled areas that increased the surface roughness with respect to the SB series. The indentations were even more accentuated for HT + SP specimens, as confirmed by quantitative roughness data. This result was potentially promoted by the higher deformability of the softened heat treated material with respect to the AB one. No statistically significant difference was detected for the surface roughness of SB and HT + SB series, probably due to the limited kinetic energy of the sand blasting treatment. HT + SP surface indentations appeared to be larger and more numerous than those of HT + SB specimens. In general, regardless the surface dimples, the surface treated specimens represented a more regular surface morphology compared to the AB and HT series.

The intrinsically high cooling rate of SLM process results in a very fine grain structure, leading to typically higher hardness with respect to those obtainable with conventional manufacturing techniques, as reported in Fig. 7a. Shot peening application on AB specimens, resulted in higher surface microhardness and deeper affected layer thanks to the higher kinetic energy compared to sand blasting. The heat treatment induced grain coarsening and thus, considerably reduced the microhardness to values comparable to the cast material [51]. Accordingly, deeper work hardening penetration in HT + SB and HT + SP specimens with respect to the SB and SP series was observed. These surface treatments and the extension of their effect are quite sensitive to the relative hardness of the impacting media with respect to the hardness of the treated material; that is a higher difference between shot-substrate hardness can result in higher extent of work hardening [68]. It is worth to note that the heat treated series represented less data scatter compared to the other specimens, which can be a result of microstructural homogenization after heat treatment.

The in-depth profile of residual stresses and FWHM parameter were extracted from the XRD analysis through a path perpendicular to the build direction. Tensile residual stresses measured in AB series can be detrimental for mechanical performance as they might cause part distortion and facilitate crack initiation. Therefore, the heat treatment, which released the residual stress can be of high impact particularly for fatigue strength enhancement. The applied surface treatments are known to induce compressive residual stresses, which is recognized to reduce the crack propagation rate and thus benefit the fatigue performance. Since the surface is more prone to fatigue crack nucleation under rotating bending fatigue loading, the induced compressive residual stresses can exhibit a key role in fatigue life enhancement. As expected, the extent of compressive stresses was higher in SP specimens compared to the SB ones. Nevertheless, the sand blasting treatment applied herein is generally stricter than the standard treatment normally used in the industry for the sole purpose of scale removal, and thus resulted in a rather deep layer affected by compressive residual stresses. Deceased hardness of the heat treated series, resulted in notable differences between the residual stress profile of the SB-SP pair and those of HT + SB and HT + SP series regarding the affected depth and the compressive peak stress.

FWHM, as a cumulative index of hardness and grain structure, reduced after heat treatment due to the increased grain size and the notably reduced hardness [51]. FWHM is known to be sensitive to the variation in microstructure and stress–strain accumulation in the material. Being related to grain distortion, dislocation density, crystallite size and residual stresses, FWHM can provide important information about the state of the material [69]. Apart from grain refinement, increased stacking faults and structural disorder as well as increased hardness and point defects density are reported to widen the XRD peak and consequently increase FWHM [70,71]. In our case, the application of mechanical surface treatments induced higher FWHM close to the surface, which decreased gradually getting close to the core material parameters. This in-depth decline was swifter for SB specimens compared to the SP ones, caused by the lower kinetic energy of sand blasting treatment. When applied after heat treatment, the surface treatments resulted in lower surface FWHM; nonetheless, they demonstrated a deeper layer characterized by higher FWHM compared to the core material. This can be due to the grain coarsening and the reduced hardness of the heat treated material, which promoted the work hardening procedure.

The AB specimens without any post treatment exhibited quite poor fatigue strength that was much lower compared to the cast and wrought material. This observation suggests that the cracks nucleated easily because of the high surface roughness and subsurface pores and propagated rapidly leading to a premature failure due to the quite limited ductility combined with the presence of tensile residual stresses. Kempen et al. [37], also confirmed the presence of borderline porosity that acted as crack initiation sites in Z-oriented SLM specimens. The fractography observations of AB specimens indicated that the high surface roughness that characterized the AB series, led to multiple crack nucleation sites, which propagated in a stable manner until the remaining cross section could not tolerate the applied stress and hence the final fracture occurred on a non-planar final fracture surface formed by coalescence of multiple crack propagations. Higher area of stable propagation zone compared to the final fracture area, which was observed on all AB specimens, is a sign of the premature failure at relatively low stresses.

The T6 heat treatment led to a considerable fatigue strength improvement, even though the porosity measurements revealed slightly higher porosity for HT specimens compared to the AB ones. Thus, it can be deduced that the synergistic effects of increased ductility, elimination of tensile residual stresses and the microstructural homogenization can increase the capacity of material to sustain the presence of a cracks, overshadowing the detrimental effect of the increased porosity. However, the obtained fatigue strength after heat treatment was still lower than average strength of the conventionally manufactured materials. Fractography observations indicated a vast unstable crack propagation region, which is correlated with higher failure stresses for the HT specimens compared to the AB ones. This observation highlights an extended crack propagation stage that is supposed to be the leading cause of fatigue performance enhancement after heat treatment.

Sand blasting and shot peening led to considerably higher fatigue strengths compared to AB series. Application of surface treatments resulted in reduced surface roughness inducing a more homogeneous surface morphology and caused quite high compressive residual stresses in the sub-surface layer. The collective effect of the aforementioned factors resulted in a much higher fatigue strength for SB and SP series compared to the cast and wrought material. Decreased surface roughness, slight closure of surface pores and the surface work hardening can contribute to retard nucleation; while compressive residual stresses together with increased ductility and microstructural homogenization can slow down crack propagation. Despite higher surface roughness of SP specimens, they demonstrated the highest obtained fatigue strength improvement. This can be the distinct effect of deeper layer with compressive residual stresses caused by shot peening.

It is worth noting that while comparing fatigue strength of SLM parts, the intrinsic anisotropy of the SLM material considering the fabrication process parameters should be taken into account, as it can affect the fatigue strength in an orientation and location wise manner [72].

Fracture surface observations revealed that the predominant failure mechanism in all SB specimens was subsurface fatigue crack initiation, which propagated around an internal pore forming the so-called fish-eye crack. This observation can imply that the presence of the compressive residual stresses successfully shifted the crack initiation site to the sub-surface layer for SB series. However, regarding SP series, the effect of surface roughness seemed to be more significant. Moreover, taking the stress gradient caused by the bending and the higher depth of residual stresses in SP specimens in to account, it is possible to argue that the surface becomes the most critical region for crack initiation site in these series. Inclined fracture surfaces observed for this series could be attributed to more than one dominant crack, which propagated on different planes.

Application of sand blasting and shot peening after heat treatment also improved the fatigue strength compared to the HT series and the conventionally manufactured material; however, the surface treatment led to lower percentage of fatigue strength improvement compared to when applied to as built material (respectively, 246% and 270% fatigue strength improvement for SB and SP compared to AB vs. 133% and 36% fatigue strength improvement for HT + SB and HT + SP compared to HT).

SB and HT + SB specimens held similar surface roughness and residual stress profile, while HT + SB specimens had higher porosity, more homogeneous microstructure, lower ultimate tensile strength and higher ductility. The compromise between these characteristics could have yielded quite similar fatigue strength for both sand blasted series. More remarkably, HT + SP series presented even reduced fatigue strength compared to the SP series. A closer observation of surface and sub-surface layer of HT + SB and HT + SP specimens revealed the main cause of their lower than expected fatigue performance. Both series represented multiple surface defects caused by the impact of media that could promote premature crack nucleation (Fig. 9). In case of HT + SB specimens, the surface defects caused the cracks to mostly initiate from surface contrary to sub-surface nucleation of SB series. Regarding shot peened series, although cracks nucleated from the surface both in SP and HT + SP configuration, the crack nucleation was further promoted by the presence of evident surface defects for HT + SP series, as the size and density of surface defects were found to be higher for HT

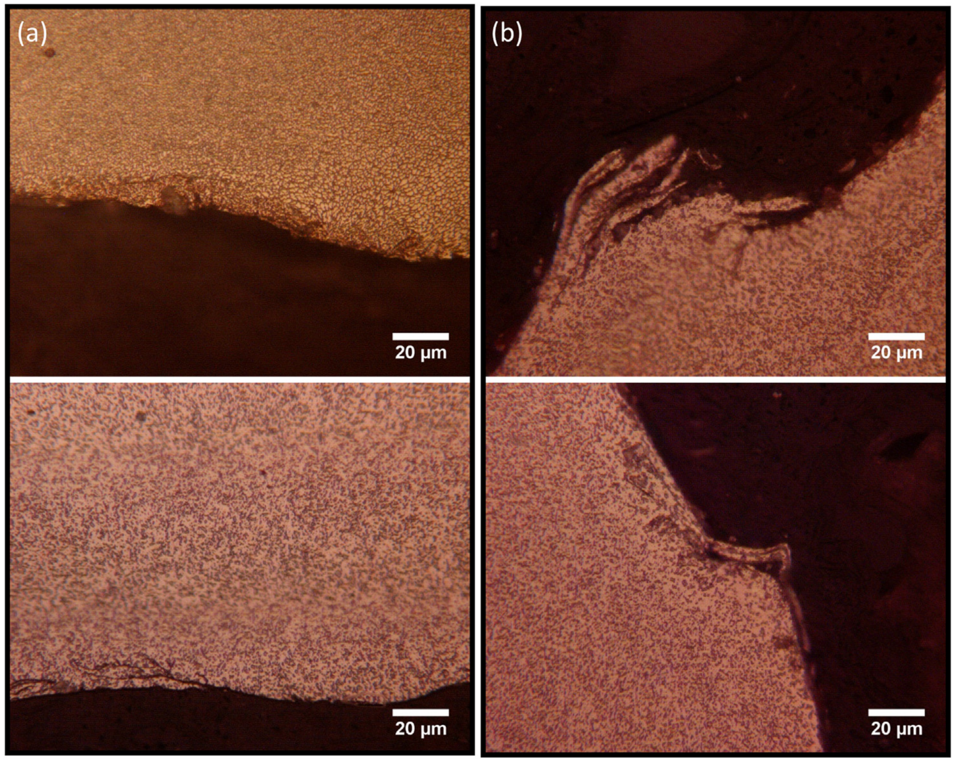

Fig. 9. Optical microscope observation of surface defects and craters for a) HT + SB and b) HT + SP specimens (HT + SB: heat treated and sand blasted, HT + SP: heat treated and shot peened).

+ SP specimens, compared to the HT + SB ones. Representative surface defects of HT + SP series presented in Fig. 9 include folded surfaces and micro-cracks that can act as stress raisers, leading to premature crack initiation; in cases where the defects were largely extended, the cracks could just propagate from the pre-existent defects, disregarding the crack nucleation phase and thus further accelerating the fracture process. As confirmed by the fractography observations of HT + SP series, dominant cracks normally nucleated where surface defects and subsurface porosity could contribute together to locally raise the stresses.

This can be justified and explained assuming that applying the same set of shot peening parameters to the as built and heat treated material could have led to considerably different surface features. Since the kinetic energy that is transmitted by the shots to the target material is inversely proportional to the difference of hardness of the impacting media and substrate [68], the softened material after heat treatment was more prone to plastic deformation upon multiple impacts and thus higher density of more extended defects were formed on the surface of HT + SP series. This notion was verified by optical microscopy observation of near surface layer for SB and SP specimens (see Fig. S2), where minor surface defects were present on the SP specimen's surface and the SB specimens showed an almost defect-free surface.

The fractography observations revealed clearly visible scan track boundaries on the fracture surfaces that were particularly more evident in case of heat treated series. Similar observation was reported by Aboulkhair et al., [16] who indicated that regardless the microstructural homogenization, interfaces between scan tracks were still represented preferential crack propagation paths.

5. Conclusions

AlSi10Mg specimens were fabricated by selective laser melting. The individual and mutual effects of different post processing techniques including kinetic surface treatments (shot peening and sand blasting) and T6 heat treatment were investigated on mechanical, microstructural and physical properties of the samples. On the base of the obtained results the following conclusions can be drawn:

- Surface morphology observations highlighted the presence of unmolten particles and agglomerates that yielded a quite high surface roughness for as built and heat treated specimens. The as built configuration also showed an inhomogeneous microstructure characterized by the presence of laser scan tracks and columnar dendrites along the building direction. The quite high surface roughness, low ductility and tensile residual stresses resulted in low dynamic performance of the as built material, caused by multiple premature surface cracks nucleation.
- T6 heat treatment radically changed mechanical behavior of SLM fabricated specimens by promoting microstructural homogenization, heat affected zone elimination and interdendritic silicon spheroidization. Combination of the aforementioned effects together with the significantly increased ductility (400%) and relaxation of tensile residual stress, counteracted the adverse effects of reduced tensile strength (70%) and the doubled porosity on the fatigue strength of the heat treated series, resulting in at least 50% fatigue strength improvement compare to as built material.
- The mechanical kinetic surface treatments led to a smoother and more regular surface morphology, caused partial closure of pores close to the surface and induced high compressive residual stresses on the sub-surface layer. Both surface treatments notably enhanced fatigue strength when applied on either as built or heat treated configurations. Considering the higher kinetic energy of shot peening, it resulted in the highest fatigue strength improvement not only compared to as built specimens (270%) but also with respect to the conventionally manufactured wrought material (over 50%).
  However, when applied to the heat treated specimens, the high kinetic energy of the multiple impacts led to surface defect formation and thus downscaled the desirable effect of the surface treatments, particularly in case of shot peening process. We postulate that in this case the effect of a milder shot peening treatment could be

more beneficial. Further work is necessary to find out the optimal shot peening parameters for heat-treated material.

In conclusion, mechanical surface treatments, as well as suitable heat treatment, were found significantly resourceful as post processing techniques to efficiently enhance the functionality and performance of SLM specimens for structural applications under dynamic loading. In particular, to obtain simultaneous high tensile strength and fatigue strength, kinetic surface treatments can be applied without a heat treatment; whereas, they need to be combined with a proper heat treatment if ductility and high fatigue strength are required concurrently. Heat treatments can be further tailored to meet specific requirements. The kinetic surface treatments proved to be especially promising for obtaining superior performance, while eliminating the need for additional surface finishing steps that can result in inconsistent data, particularly since in most cases the pores are not regularly localized close to the surface layer.

Acknowledgement

The authors declare no conflict of interests in this work. We would like to thank Dr. Davide Mombelli for his valuable help with the heat treatment.

Data availability

All data generated or analyzed during this study are included in this published article and its supplementary information files.

Appendix A. Supplementary data

Supplementary data to this article can be found online at https://doi.org/10.1016/j.matdes.2018.02.055.

References

[1] N.T. Aboulkhair, I. Maskery, C. Tuck, I. Ashcroft, N.M. Everitt, On the formation of AlSi10Mg single tracks and layers in selective laser melting: microstructure and nano-mechanical properties, J. Mater. Process. Technol. 230 (2016) 88–98.
[2] D.D. Deligianni, N.D. Katsala, P.G. Koutsoukos, Y.F. Missirlis, Effect of surface rough-ness of hydroxyapatite on human bone marrow cell adhesion, proliferation, differ-entiation and detachment strength, Biomaterials 22 (2000) 87–96.
[3] S. Bagherifard, D.J. Hickey, A.C. de Luca, V.N. Malheiro, A.E. Markaki, M. Guagliano, et al., The influence of nanostructured features on bacterial adhesion and bone cell functions on severely shot peened 316L stainless steel, Biomaterials 73 (2015) 185–197.
[4] S. Bagherifard, D.J. Hickey, S. Fintová, F. Pastorek, I. Fernandez-Pariente, M. Bandini, et al., Effects of nanofeatures induced by severe shot peening (SSP) on mechanical, corrosion and cytocompatibility properties of magnesium alloy AZ31, Acta Biomater. 66 (2018) 93–108.
[5] Y. Kok, X.P. Tan, P. Wang, M.L.S. Nai, N.H. Loh, E. Liu, et al., Anisotropy and heteroge-neity of microstructure and mechanical properties in metal additive manufacturing: a critical review, Mater. Des. 139 (2018) 565–586.
[6] W.E. Frazier, Metal additive manufacturing: a review, J. Mater. Eng. Perform. 23 (2014) 1917–1928.
[7] A. Townsend, N. Senin, L. Blunt, R.K. Leach, J.S. Taylor, Surface texture metrology for metal additive manufacturing: a review, Precis. Eng. 46 (2016) 34–47.
[8] E. Brandl, U. Heckenberger, V. Holzinger, D. Buchbinder, Additive manufactured AlSi10Mg samples using selective laser melting (SLM): microstructure, high cycle fatigue, and fracture behavior, Mater. Des. 34 (2012) 159–169.
[9] L. Hitzler, C. Janousch, J. Schanz, M. Merkel, F. Mack, A. Öchsner, Non-destructive evaluation of AlSi10Mg prismatic samples generated by selective laser melting: in-fluence of manufacturing conditions, Mater. Werkst. 47 (2016) 564–581.
[10] G. Strano, L. Hao, R.M. Everson, K.E. Evans, Surface roughness analysis, modelling and prediction in selective laser melting, J. Mater. Process. Technol. 213 (2013) 589–597.
[11] F. Calignano, D. Manfredi, E. Ambrosio, L. Iuliano, P. Fino, Influence of process param-eters on surface roughness of aluminum parts produced by DMLS, Int. J. Adv. Manuf. Technol. 67 (2013) 2743–2751.
[12] K. Mumtaz, N. Hopkinson, Top surface and side roughness of Inconel 625 parts proc-essed using selective laser melting, Rapid Prototyp. J. 15 (2009) 96–103.
[13] B. Song, S. Dong, B. Zhang, H. Liao, C. Coddet, Effects of processing parameters on mi-crostructure and mechanical property of selective laser melted Ti6Al4V, Mater. Des. 35 (2012) 120–125.
[14] A. Yadollahi, N. Shamsaei, Additive manufacturing of fatigue resistant materials: challenges and opportunities, Int. J. Fatigue 98 (2017) 14–31.
[15] A. Fortunato, A. Lulaj, S. Melkote, E. Liverani, A. Ascari, D. Umbrello, Milling of maraging steel components produced by selective laser melting, Int. J. Adv. Manuf. Technol. 94 (5–8) (2018) 1895–1902.
[16] N.T. Aboulkhair, I. Maskery, C. Tuck, I. Ashcroft, N.M. Everitt, Improving the fatigue behaviour of a selectively laser melted aluminium alloy: influence of heat treatment and surface quality, Mater. Des. 104 (2016) 174–182.
[17] S. Bagehorn, T. Mertens, D. Greitemeier, L. Carton, A. Schoberth, Surface finishing of additive manufactured Ti-6Al-4V—a comparison of electrochemical and mechanical treatments, 6th Eur. Conf. Aerosp. Sci. (2015).
[18] S.-M.-J. Razavi, P. Ferro, F. Berto, Fatigue assessment of Ti–6Al–4V circular notched specimens produced by selective laser melting, Metals 7 (2017) 291.
[19] J. Guo, J. Bai, K. Liu, J. Wei, Surface quality improvement of selective laser sintered polyamide 12 by precision grinding and magnetic field-assisted finishing, Mater. Des. 138 (2018) 39–45.
[20] B. Rosa, P. Mognol, J.-Y. Hascoët, Laser polishing of additive laser manufacturing sur-faces, Journal of Laser Applications 27 (2015), S29102.
[21] K. Alrbaey, D. Wimpenny, R. Tosi, W. Manning, A. Moroz, On optimization of surface roughness of selective laser melted stainless steel parts: a statistical study, J. Mater. Eng. Perform. 23 (2014) 2139–2148.
[22] J. Schanz, M. Hofele, S. Ruck, T. Schubert, L. Hitzler, G. Schneider, et al., Metallurgical investigations of laser remelted additively manufactured AlSi10Mg parts, Mater. Werkst. 48 (2017) 463–476.
[23] Z. Baicheng, L. Xiaohua, B. Jiaming, G. Junfeng, W. Pan, S. Chen-nan, et al., Study of selective laser melting (SLM) Inconel 718 part surface improvement by electro-chemical polishing, Mater. Des. 116 (2017) 531–537.
[24] T.M. Mower, M.J. Long, Mechanical behavior of additive manufactured, powder-bed laser-fused materials, Mater. Sci. Eng. A 651 (2016) 198–213.
[25] S. Bagherifard, R. Ghelichi, M. Guagliano, On the shot peening surface coverage and its assessment by means of finite element simulation: a critical review and some original developments, Appl. Surf. Sci. 259 (2012) 186–194.
[26] I. Fernández-Pariente, S. Bagherifard, M. Guagliano, R. Ghelichi, Fatigue behavior of nitrided and shot peened steel with artificial small surface defects, Eng. Fract. Mech. 103 (2013) 2–9.
[27] S. Bagherifard, I. Fernandez-Pariente, R. Ghelichi, M. Guagliano, Fatigue behavior of notched steel specimens with nanocrystallized surface obtained by severe shot peening, Mater. Des. 45 (2013) 497–503.
[28] J. González, S. Bagherifard, M. Guagliano, I.F. Pariente, Influence of different shot peening treatments on surface state and fatigue behaviour of Al 6063 alloy, Eng. Fract. Mech. 185 (2017) 72–81.
[29] S.B. Fard, M. Guagliano, Effects of surfaces nanocrystallization induced by shot peening on material properties: a review, Frattura ed Integrità Strutturale: Annals 2010 (2009) 3.
[30] S. Bagherifard, C. Colombo, M. Guagliano, Application of different fatigue strength criteria to shot peened notched components. Part 1: fracture mechanics based ap-proaches, Appl. Surf. Sci. 289 (2014) 180–187.
[31] Committee AIH, ASM Handbook: Heat Treating, Asm Intl, 1991.
[32] J.L. Dossett, H.E. Boyer, Practical Heat Treating, Asm International, 2006.
[33] P. Ma, K.G. Prashanth, S. Scudino, Y. Jia, H. Wang, C. Zou, et al., Influence of annealing on mechanical properties of Al-20Si processed by selective laser melting, Metals 4 (2014) 28–36.
[34] K. Prashanth, S. Scudino, H. Klauss, K.B. Surreddi, L. Löber, Z. Wang, et al., Microstruc-ture and mechanical properties of Al–12Si produced by selective laser melting: ef-fect of heat treatment, Mater. Sci. Eng. A 590 (2014) 153–160.
[35] N. Takata, H. Kodaira, K. Sekizawa, A. Suzuki, M. Kobashi, Change in microstructure of selectively laser melted AlSi10Mg alloy with heat treatments, Mater. Sci. Eng. A 704 (2017) 218–228.
[36] L. Hitzler, J. Hirsch, B. Heine, M. Merkel, W. Hall, A. Öchsner, On the anisotropic me-chanical properties of selective laser-melted stainless steel, Materials 10 (2017) 1136.
[37] K. Kempen, L. Thijs, J. Van Humbeeck, J.-P. Kruth, Mechanical properties of AlSi10Mg produced by selective laser melting, Phys. Procedia 39 (2012) 439–446.
[38] D. Manfredi, F. Calignano, M. Krishnan, R. Canali, E.P. Ambrosio, E. Atzeni, From pow-ders to dense metal parts: characterization of a commercial AlSiMg alloy processed through direct metal laser sintering, Materials 6 (2013) 856–869.
[39] S. Siddique, M. Imran, M. Rauer, M. Kaloudis, E. Wycisk, C. Emmelmann, et al., Com-puted tomography for characterization of fatigue performance of selective laser melted parts, Mater. Des. 83 (2015) 661–669.
[40] S. Beretta, S.A. Romano, Comparison of fatigue strength sensitivity to defects for ma-terials manufactured by AM or traditional processes, Int. J. Fatigue 94 (2017) 178–191.
[41] T.A. Book, M.D. Sangid, Evaluation of select surface processing techniques for in situ application during the additive manufacturing build process, JOM 68 (2016) 1780–1792.
[42] B. AlMangour, J.-M. Yang, Improving the surface quality and mechanical properties by shot-peening of 17-4 stainless steel fabricated by additive manufacturing, Mater. Des. 110 (2016) 914–924.
[43] S. Bagherifard, I. Fernandez-Pariente, R. Ghelichi, M. Guagliano, Severe shot peening to obtain nanostructured surfaces: process and properties of the treated surfaces, Handbook of Mechanical Nanostructuring (2015) 299–323.
[44] S. Bagherifard, R. Ghelichi, M. Guagliano, A numerical model of severe shot peening (SSP) to predict the generation of a nanostructured surface layer of material, Surf. Coat. Technol. 204 (2010) 4081–4090.
[45] S. Bagherifard, M. Guagliano, Fatigue behavior of a low-alloy steel with nanostruc-tured surface obtained by severe shot peening, Eng. Fract. Mech. 81 (2012) 56–68.

[46] E. Wycisk, C. Emmelmann, S. Siddique, F. Walther, High cycle fatigue (HCF) perfor-mance of Ti-6Al-4V alloy processed by selective laser melting, Adv. Mater. Res.: Trans. Tech. Publ. (2013) 134–139.
[47] D. Manfredi, F. Calignano, M. Krishnan, R. Canali, E.P. Ambrosio, S. Biamino, et al., Ad-ditive manufacturing of Al alloys and aluminium matrix composites (AMCs), Light Metal Alloys Applications, InTech, 2014.
[48] D. Buchbinder, W. Meiners, K. Wissenbach, R. Poprawe, Selective laser melting of aluminum die-cast alloy—correlations between process parameters, solidification conditions, and resulting mechanical properties, Journal of Laser Applications 27 (2015), S29205.
[49] L. Hitzler, J. Hirsch, J. Schanz, B. Heine, M. Merkel, W. Hall, et al., Fracture toughness of selective laser melted AlSi10Mg, Proc. Inst. Mech. Eng. L. J. Mater. Des. Appl.(2017), 1464420716687337.
[50] M. Shiomi, K. Osakada, K. Nakamura, T. Yamashita, F. Abe, Residual stress within me-tallic model made by selective laser melting process, CIRP Annals-Manufacturing Technology 53 (2004) 195–198.
[51] N.T. Aboulkhair, I. Maskery, C. Tuck, I. Ashcroft, N.M. Everitt, The microstructure and mechanical properties of selectively laser melted AlSi10Mg: the effect of a conven-tional T6-like heat treatment, Mater. Sci. Eng. A 667 (2016) 139–146.
[52] F. Gharavi, K.A. Matori, R. Yunus, N.K. Othman, Corrosion behavior of friction stir welded lap joints of AA6061-T6 aluminum alloy, Mater. Res. 17 (2014) 672–681.
[53] C.A. Schneider, W.S. Rasband, K.W. Eliceiri, NIH image to ImageJ: 25 years of image analysis, Nat. Methods 9 (2012) 671–675.
[54] W.J. Dixon, F.J. Massey Jr., Introduction to Statistical Analysis, 3rd ed. McGraw-Hill Book Co, New York, 1969 61:1l.
[55] K. Brownlee, J. Hodges Jr., M. Rosenblatt, The up-and-down method with small sam-ples, J. Am. Stat. Assoc. 48 (1953) 262–277.
[56] N.T. Aboulkhair, C. Tuck, I. Ashcroft, I. Maskery, N.M. Everitt, On the precipitation hardening of selective laser melted AlSi10Mg, Metall. Mater. Trans. A 46 (2015) 3337–3341.
[57] Z. Wang, K. Guan, M. Gao, X. Li, X. Chen, X. Zeng, The microstructure and mechanical properties of deposited-IN718 by selective laser melting, J. Alloys Compd. 513 (2012) 518–523.
[58] S. Bagherifard, S. Slawik, I. Fernández-Pariente, C. Pauly, F. Mücklich, M. Guagliano, Nanoscale surface modification of AISI 316L stainless steel by severe shot peening, Mater. Des. 102 (2016) 68–77.
[59] B. Atzori, G. Meneghetti, L. Susmel, Fatigue behaviour of AA356-T6 cast aluminium alloy weakened by cracks and notches, Eng. Fract. Mech. 71 (2004) 759–768.
[60] M. Tang, P.C. Pistorius, Oxides, porosity and fatigue performance of AlSi10Mg parts produced by selective laser melting, Int. J. Fatigue 94 (Part 2) (2017) 192–201.
[61] J.G. Kaufman, Properties of Aluminum Alloys: Fatigue Data and the Effects of Tem-perature, Product Form, and Processing, ASM International, 2008.
[62] F. Trevisan, F. Calignano, M. Lorusso, J. Pakkanen, A. Aversa, E.P. Ambrosio, et al., On the selective laser melting (SLM) of the AlSi10Mg alloy: process, microstructure, and mechanical properties, Materials 10 (2017) 76.
[63] S. Siddique, M. Imran, F. Walther, Very high cycle fatigue and fatigue crack propaga-tion behavior of selective laser melted AlSi12 alloy, Int. J. Fatigue 94 (2017) 246–254.
[64] I. Rosenthal, A. Stern, N. Frage, Microstructure and mechanical properties of AlSi10Mg parts produced by the laser beam additive manufacturing (AM) technol-ogy, Metallography, Microstructure, and Analysis 3 (2014) 448–453.
[65] A.I. Mertens, J. Delahaye, J. Lecomte-Beckers, Fusion-based additive manufacturing for processing aluminum alloys: state-of-the-art and challenges, Adv. Eng. Mater. 19 (8) (2017), 1700003. https://doi.org/10.1002/adem.201700003.
[66] D. Manfredi, E. Ambrosio, F. Calignano, M. Krishnan, R. Canali, S. Biamino, et al., Di-rect metal laser sintering: an additive manufacturing technology ready to produce lightweight structural parts for robotic applications, La Metallurgia Italiana 10 (2013).
[67] S. Bagherifard, I. Fernandez-Pariente, R. Ghelichi, M. Guagliano, Effect of severe shot peening on microstructure and fatigue strength of cast iron, Int. J. Fatigue 65 (2014) 64–70.
[68] F.-X. Abadie, Shot Peening: A Dynamic Application and its Future, MFN Publishing House, 2009.
[69] I.C. Noyan, J.B. Cohen, Residual Stress: Measurement by Diffraction and Interpreta-tion, Springer, 2013.
[70] J.-M. Kim, H.-T. Chung, Electrochemical characteristics of orthorhombic $LiMnO_2$ with different degrees of stacking faults, J. Power Sources 115 (2003) 125–130.
[71] H.-M. Tung, J.-H. Huang, D.-G. Tsai, C.-F. Ai, G.-P. Yu, Hardness and residual stress in nanocrystalline ZrN films: effect of bias voltage and heat treatment, Mater. Sci. Eng. A 500 (2009) 104–108.
[72] L. Hitzler, C. Janousch, J. Schanz, M. Merkel, B. Heine, F. Mack, et al., Direction and lo-cation dependency of selective laser melted AlSi10Mg specimens, J. Mater. Process. Technol. 243 (2017) 48–61.